Contents lists available at ScienceDirect

Physics Letters B

www.elsevier.com/locate/physletb

PHYSICS LETTERS B

Transverse momentum spectra of charged particles in proton–proton collisions at $\sqrt{s} = 900$ GeV with ALICE at the LHC [☆],[☆☆]

ALICE Collaboration

A B S T R A C T

The inclusive charged particle transverse momentum distribution is measured in proton–proton collisions at $\sqrt{s} = 900$ GeV at the LHC using the ALICE detector. The measurement is performed in the central pseudorapidity region ($|\eta| < 0.8$) over the transverse momentum range $0.15 < p_T < 10$ GeV/c. The correlation between transverse momentum and particle multiplicity is also studied. Results are presented for inelastic (INEL) and non-single-diffractive (NSD) events. The average transverse momentum for $|\eta| < 0.8$ is $\langle p_T \rangle_{\mathrm{INEL}} = 0.483 \pm 0.001$ (stat.) ± 0.007 (syst.) GeV/c and $\langle p_T \rangle_{\mathrm{NSD}} = 0.489 \pm 0.001$ (stat.) ± 0.007 (syst.) GeV/c, respectively. The data exhibit a slightly larger $\langle p_T \rangle$ than measurements in wider pseudorapidity intervals. The results are compared to simulations with the Monte Carlo event generators PYTHIA and PHOJET.

2010 Published by Elsevier B.V. Open access under CC BY-NC-ND license.

1. Introduction

The precise measurement of the transverse momentum spectrum of charged particles produced in proton collisions in the energy range of the Large Hadron Collider (LHC) [1] offers unique information about soft and hard interactions. Perturbative Quantum Chromodynamics (pQCD) is a framework for the quantitative description of parton–parton interactions at large momentum transfers, i.e. hard scattering processes. However, a significant fraction of the particles produced in *pp* collisions do not originate from hard interactions, even at LHC energies. In contrast to hard processes, the description of particle production in soft interactions is not well-established within QCD. Current models of hadron–hadron collisions at high energies, such as the event generators PYTHIA [2] and PHOJET [3], combine perturbative QCD for the description of hard parton interactions with phenomenological approaches to model the soft component of the produced particle spectrum. Data on charged particle production in hadron–hadron collisions will have to be used to tune these models before they can provide a detailed description of the existing measurements and predictions for particle production characteristics in *pp* collisions at the highest LHC energies. These data include the measurement of multiplicity, pseudorapidity (η) and transverse momentum (p_T) distributions of charged particles and correlations, such as the dependence of the average transverse momentum, $\langle p_T \rangle$, on the charged particle multiplicity.

The charged particle pseudorapidity densities and multiplicity distributions in *pp* collisions at $\sqrt{s} = 0.9$, 2.36 and 7 TeV were presented in recent publications by the ALICE Collaboration [4–6]. In this Letter, we present a measurement in *pp* collisions at $\sqrt{s} = 900$ GeV of the transverse momentum spectrum of primary charged particles and the correlation between $\langle p_T \rangle$ and the charged particle multiplicity. Primary particles include particles produced in the collision or their decay products, except those from weak decays of strange hadrons. The measurement is performed in the central rapidity region ($|\eta| < 0.8$) and covers a p_T range $0.15 < p_T < 10$ GeV/c, where both hard and soft processes are expected to contribute to particle production. The data from the ALICE experiment presented in this Letter serve as a baseline for future studies of *pp* collisions at higher LHC energies and particle production in heavy-ion collisions [7].

2. Experiment and data collection

The data were collected with the ALICE detector [8] during the startup phase of the LHC in December 2009. The ALICE detector, designed to cope with high track densities in heavy-ion collisions, provides excellent track reconstruction and particle identification capabilities. This also makes the detector well-suited to detailed studies of global characteristics of pp interactions [7].

In this analysis of the first pp collisions at $\sqrt{s} = 900$ GeV, charged particle tracking and momentum reconstruction are based on data recorded with the Time Projection Chamber (TPC) and the Inner Tracking System (ITS), both located in the central barrel of ALICE. The detectors in the central barrel are operated inside a large solenoidal magnet providing a uniform 0.5 T field.

The ALICE TPC [9] is a large cylindrical drift detector with a central high voltage membrane maintained at -100 kV and two readout planes at the end-caps. The active volume is limited to $85 < r < 247$ cm and $-250 < z < 250$ cm in the radial and longitudinal directions respectively. The material budget between the interaction point and the active volume of the TPC corresponds to 11% of a radiation length, averaged in $|\eta| < 0.8$. The central membrane at $z = 0$ divides the nearly 90 m^3 active volume into two halves. The homogeneous drift field of 400 V/cm in the Ne–CO$_2$–N$_2$ (85.7%–9.5%–4.8%) gas mixture leads to a maximum drift time of 94 μs. Ionization electrons produced by charged particles traversing the TPC drift towards the readout end-caps composed of 72 multi-wire proportional chambers with cathode pad readout. The typical gas gain is 10^4. Signals induced on the segmented cathode planes, comprising a total of 558k readout pads, are transformed into differential semi-Gaussian signals by a charge-sensitive shaping amplifier (PASA). This is followed by the ALICE TPC ReadOut (ALTRO) chip, which employs a 10 bit ADC at 10 MHz sampling rate and four digital filtering circuits. These filters also perform tail cancellation and baseline restoration. They are optimized for precise position and dE/dx measurements in the high track density environment of heavy-ion collisions. To ensure optimal drift and charge transport properties, the TPC was operated with an overall temperature uniformity of $\Delta T \approx 60$ mK (r.m.s.). The oxygen contamination was less than 5 ppm.

The ITS is composed of high resolution silicon tracking detectors, arranged in six cylindrical layers at radial distances to the beam line from 3.9 to 43 cm. Three different technologies are employed.

For the two innermost layers Silicon Pixel Detectors (SPD) are used, covering the pseudorapidity ranges $|\eta| < 2$ and $|\eta| < 1.4$, respectively. A total of 9.8 million 50×425 μm^2 pixels enable the reconstruction of the primary event vertex and the track impact parameters with high precision. The SPD was also included in the trigger scheme for data collection.

The SPD is followed by two Silicon Drift Detector (SDD) layers with a total of 133k readout channels, sampling the drift time information at a frequency of 20 MHz. The SDD are operated with a drift field of 500 V/cm, resulting in a drift speed of about 6.5 μm/ns and in a maximum drift time of about 5.3 μs.

The two outermost Silicon Strip Detector (SSD) layers consist of double-sided silicon micro-strip sensors with 95 μm pitch, comprising a total of 2.6 million readout channels. Strips of the two sensor sides form a stereo angle of 35 mrad, providing two-dimensional hit reconstruction.

The design spatial resolutions of the ITS sub-detectors ($\sigma_{r\phi} \times \sigma_z$) are: 12×100 μm^2 for SPD, 35×25 μm^2 for SDD, and 20×830 μm^2 for SSD. The SPD and SSD detectors were aligned using survey measurements, cosmic muon data [10] and collision data to an estimated accuracy of 10 μm for the SPD and 15 μm for the SSD. No alignment corrections are applied to the positions of the SDD modules, for which calibration and alignment are in progress. The estimated misalignment of the SDD modules is about 100 μm. The TPC and ITS are aligned relative to each other to the level of a few hundred micrometers using cosmic-ray and pp data by comparing pairs of track segments independently reconstructed in the two detectors.

The two forward scintillator hodoscopes (VZERO) are included in the trigger. Each detector is segmented into 32 scintillator counters which are arranged in four rings around the beam pipe. They are located at distances $z = 3.3$ m and $z = -0.9$ m from the nominal interaction point and cover the pseudorapidity ranges: $2.8 < \eta < 5.1$ and $-3.7 < \eta < -1.7$ respectively. The time resolution of about 1 ns of the VZERO hodoscope also allows for a discrimination against beam-gas interactions.

During the startup phase of the LHC in 2009, four proton bunches per beam were circulating in the LHC with two pairs of bunches crossing at the ALICE intersection region and protons colliding at $\sqrt{s} = 900$ GeV. The detector readout was triggered using the LHC bunch-crossing signals in coincidence with signals from the two upstream beam pick-up counters and a minimum-bias interaction trigger requiring a signal in at least one of the SPD pixels or one of the VZERO counters [4,5]. Events with only one bunch or no bunches passing through ALICE were also recorded to study beam related and random background.

3. Data analysis

The total inelastic pp cross section is commonly subdivided into contributions from diffractive and non-diffractive processes. To facilitate comparison with existing measurements, we perform our analysis for two classes of events: inelastic (INEL) and non-single-diffractive (NSD) pp collisions.

In this analysis, 3.44×10^5 triggered pp events at $\sqrt{s} = 900$ GeV are analyzed. To remove beam related background events, an offline event selection based on the VZERO timing signal and the correlation between the number of hits and tracklets in the SPD is applied as in [5], reducing the sample to 2.67×10^5 events. This event selection is referred to as MB$_{OR}$ [5].

For the INEL analysis we use the event sample selected with the MB$_{OR}$ condition. A subset of these events (2.15×10^5) is used for the NSD analysis, selected offline by requiring a coincidence between the two VZERO detectors (the MB$_{AND}$ selection). This condition suppresses a significant fraction of the single-diffractive events and hence reduces the systematic errors related to model dependent corrections [5].

The fractions of the different process types contributing to the selected event samples are estimated by a Monte Carlo simulation, implementing a description of the ALICE detector response [11] to pp collisions at $\sqrt{s} = 900$ GeV from the PYTHIA event generator version 6.4.21 tune D6T (109) [12]. The process fractions of single-diffractive (SD) and double-diffractive (DD) events are scaled in Monte Carlo to match the cross sections in $p\bar{p}$ at $\sqrt{s} = 900$ GeV measured by UA5 [13]. The selection efficiency for INEL events using MB$_{OR}$ and NSD events using MB$_{AND}$ is approximately 96% and 93%, respectively [5].

Charged particle tracks are reconstructed using information from the TPC and ITS detector systems. Signals on adjacent pads in the TPC are connected to particle tracks by employing a Kalman filter algorithm. The TPC tracks are extrapolated to the ITS and matching hits in the ITS detector layers are assigned to the track. In order to maximize the hit matching efficiency and avoid possible biases of the track parameters due to the non-uniform degree of alignment of the ITS sub-detectors, the space point uncertainties of the ITS hits are set to 100 μm for SPD and 1 mm for both SDD and SSD.

The event vertex is reconstructed using the combined track information from TPC and ITS. The tracks are extrapolated to the intersection region and the position of the event vertex is fitted, using the measured average intersection profile as a constraint. The profile of the intersection region is determined on a run-by-run basis in a first pass through the data using the mean and the spread of the distribution of the reconstructed vertices. The event vertex distribution is found to be Gaussian with standard deviations of approximately 210 μm, 250 μm, and 4.1 cm, along x, y (transverse to the beam-axis) and z respectively. For events where only one track is found, the vertex is determined from the point of closest approach of the track to the beam axis. If no track is found in the TPC, the event vertex reconstruction is based on tracklets built by associating pairs of hits of the two innermost ITS layers (SPD). An event with a reconstructed vertex position z_v is accepted if $|z_v - z_0| < 10$ cm, corresponding to about 2.5 standard deviations of the reconstructed event vertex distribution centered at z_0 [5].

The vertex position resolution depends on the event multiplicity. It can be parametrized as 540 μm/$(N_{SPD})^{0.45}$ in x and y, and 550 μm/$(N_{SPD})^{0.6}$ in z, where N_{SPD} corresponds to the number of SPD tracklets. This resolution is consistent with Monte Carlo simulations. The probability of multiple interactions in the same bunch crossing (pile-up) in the present data set is 10^{-4} and therefore neglected.

The fraction of selected events in the MB$_{OR}$ (MB$_{AND}$) sample where an event vertex is successfully reconstructed is 80% (92%), resulting in a sample of 2.13×10^5 INEL (1.98×10^5 NSD) events used in the present analysis. Events, where no vertex is found, are included when normalizing the results. In order to understand and to subtract possible beam-induced background, the detector was also triggered on bunches coming from either side of the interaction region, but not colliding with another bunch. From the study of these events we estimate that 21% of the triggered MB$_{OR}$ and MB$_{AND}$ events without a reconstructed event vertex or with zero selected tracks are background, and the number of events used for normalization of the final results is corrected accordingly. The estimated contribution from beam-induced background events to the event sample, where a vertex was found, is negligible. From the analysis of empty bunch crossing events the random contribution from cosmics and noise triggers is also found to be negligible.

To study the transverse momentum spectrum, charged particle tracks are selected in the pseudorapidity range $|\eta| < 0.8$. In this range, tracks in the TPC can be reconstructed with maximal length, and there are minimal efficiency losses due to detector boundaries. Additional quality requirements are applied to ensure high tracking resolution and low secondary and fake track contamination. A track is accepted if it has at least 70 out of the maximum of 159 space points in the TPC, and the χ^2 per space point used for the momentum fit is less than 4. Additionally, at least two hits in the ITS must be associated with the track, and at least one has to be in either of the two innermost layers, i.e., in the SPD. The average number of associated hits per track in the six ITS layers is 4.7, mainly determined by the fraction of inactive channels, and is well reproduced in Monte Carlo simulations. Tracks with $p_T < 0.15$ GeV/c are excluded because their reconstruction efficiency drops below 50%. Tracks are also rejected as not associated to the primary vertex if their distance of closest approach to the reconstructed event vertex in the plane perpendicular to the beam axis, d_0, satisfies $d_0 > 0.35$ mm $+ 0.42$ mm $\times p_T^{-0.9}$, with p_T in GeV/c. This cut corresponds to about seven standard deviations of the p_T dependent transverse impact parameter resolution for primary tracks passing the above selection. It is tuned to select primary charged particles with high efficiency and to minimize the contributions from weak decays, conversions and secondary hadronic interactions in the detector material. The accepted number of charged particles per event which fulfill these conditions is called n_{acc}.

With this selection, the reconstruction efficiency for primary charged particles and the remaining contamination from secondaries as a function of p_T are estimated by Monte Carlo simulation using PYTHIA, combined with detector simulation and event reconstruction. The procedure estimates losses due to tracking inefficiency, charged particles escaping detection due to weak decay, absorption and secondary interaction in the detector. The inefficiencies of the event selection and of the event vertex reconstruction are accounted for. The latter two affect mostly low-multiplicity events, which imposes a bias on the uncorrected p_T spectrum due to the correlation between multiplicity and average momentum.

The primary charged particle track reconstruction efficiency in the region $|\eta| < 0.8$ reaches 75% at $p_T \sim 1$ GeV/c, as shown in Fig. 1. The slight decrease of efficiency observed for $p_T > 1.5$ GeV/c is a consequence of the projective segmentation of the readout plane in azimuth, causing stiff tracks to remain undetected if they fall between two adjacent TPC readout sectors. For $p_T < 0.6$ GeV/c, the reconstruction efficiency decreases and reaches 50% at 0.15 GeV/c. The losses at low p_T are mainly due to energy loss in the detector material and to the track bending in the magnetic field. No significant dependence of the track reconstruction efficiency on the track density is observed in simulations for charged particle multiplicities relevant for this analysis. The contamination from secondary particles such as charged particles from weak decays, electrons from photon conversions, and products from secondary interactions in the detector material is also shown in Fig. 1. It has a maximum of 9% at the lowest p_T and drops below 3% for $p_T > 1$ GeV/c. A comparison of the d_0 distributions of data and Monte Carlo tracks indicates that the Monte Carlo simulation using PYTHIA underestimates the particle yield from secondaries by 0–50%, depending on p_T. This is consistent with the fact that PYTHIA underestimates the strangeness yield by a similar amount, when compared to previous results in pp and $p\bar{p}$ collisions [14,15]. For the final corrections to the data we scale accordingly the contamination level obtained with PYTHIA, resulting in an additional 0–1.5% decrease of the primary particle yields. The uncertainty in the strangeness yield is taken into account in the evaluation of the overall systematic uncertainties, as discussed below.

The reconstruction efficiency and contamination are converted to p_T dependent correction factors used to correct the raw p_T spectrum. We note that efficiency and secondary contamination are slightly different for positively and negatively charged particles, mainly due to the larger absorption of negatively charged particles and isospin effects in secondary interactions.

The charged particle transverse momenta are measured in the TPC, taking into account energy loss based on the PID hypothesis from TPC dE/dx and the material budget in front of the TPC. The material budget is studied via the measurement of electron–positron pairs in the TPC from photon conversions. The radial distribution of the reconstructed photon conversion points is compared to Monte Carlo simulations. The sum of all positive and negative deviations is $+4.7\%$ and -7.2%, respectively. The remaining material budget
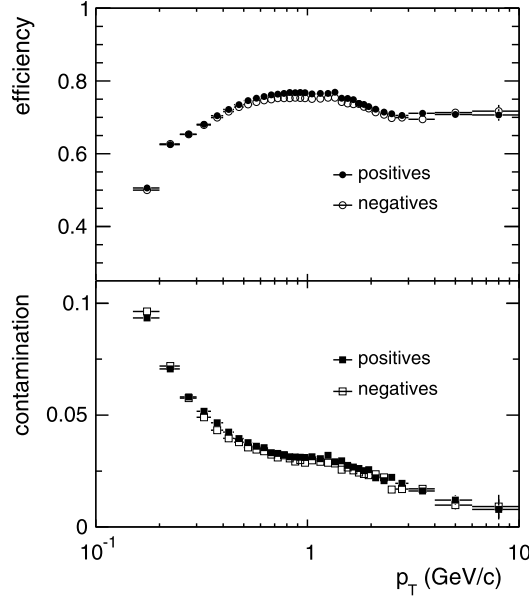
Fig. 1. Charged-particle track reconstruction efficiency for primary particles (top) and contamination from secondary particles (bottom), for positively and negatively charged particles in $|\eta| < 0.8$ as a function of p_T. The tracking efficiency is normalized to the number of generated primary particles using PYTHIA. The contamination from secondary tracks was scaled in Monte Carlo to match the measured d_0 distributions (see text).

uncertainty enters into the final systematic uncertainties. In this analysis, we use the measurement of the momentum at the event vertex.

At the present level of calibration, the transverse momentum resolution achieved in the TPC is given by $(\sigma(p_T)/p_T)^2 = (0.01)^2 + (0.007 \cdot p_T)^2$, with p_T in GeV/c. The transverse momentum resolution for $p_T > 1$ GeV/c is measured in cosmic muon events by comparing the muon momenta reconstructed in the upper and lower halves of the TPC. For $p_T < 1$ GeV/c, the Monte Carlo estimate of $\sigma(p_T)/p_T \approx 1\%$ is cross-checked using the measured K_s^0 invariant mass distribution. A Monte Carlo based correction is applied to the p_T spectra to account for the finite momentum resolution. The correction increases with p_T and reaches 1.2% at 10 GeV/c.

The calibration of the absolute momentum scale is verified employing the invariant mass spectra of Λ, $\bar{\Lambda}$, K_s^0 and ϕ. The reconstructed peak positions agree with their PDG values within 0.3 MeV/c^2. As a cross-check, the q/p_T distributions of particles with charge q in data and Monte Carlo simulation are compared and the symmetry of the minimum around $q/p_T = 0$ is studied. Based on these studies, we estimate an upper limit on the systematic uncertainty of the momentum scale of $|\Delta(p_T)/p_T| < 0.003$. Within the p_T reach of this study, the effect of the momentum scale uncertainty on the final spectra is found to be negligible.

For the normalization of the transverse momentum spectra to the number of events, multiplicity dependent correction factors are derived from the event selection and vertex reconstruction efficiencies for INEL and NSD events, evaluated with the PYTHIA Monte Carlo event generator.

The fully corrected p_T spectra are fitted by the modified Hagedorn function [16]

$$\frac{1}{2\pi p_T} \frac{d^2 N_{ch}}{d\eta \, dp_T} \propto \frac{p_T}{m_T} \left(1 + \frac{p_T}{p_{T,0}}\right)^{-b}. \tag{1}$$

For the transverse mass $m_T = \sqrt{m_\pi^2 + p_T^2}$, the pion mass is assumed for all tracks. At small p_T, the term $(1 + \frac{p_T}{p_{T,0}})^{-b}$ behaves like an exponential in p_T with inverse slope parameter $p_{T,0}/b$. This provides a good description of the soft part of the spectrum, allowing for an extrapolation of the measured data to $p_T = 0$. To assess the tail of the spectrum at $p_T > 3$ GeV/c, a power law fit is performed

$$\frac{1}{2\pi p_T} \frac{d^2 N_{ch}}{d\eta \, dp_T} \propto p_T^{-n}, \tag{2}$$

yielding a very good description of the hard part of the spectrum characterized by the power n.

The calculation of $\langle p_T \rangle$ in all INEL and NSD events is performed using the weighted average over the measured points in the range $0.15 < p_T < 10$ GeV/c combined with the result of the Hagedorn fit to extrapolate to $p_T = 0$.

In order to analyze the behaviour of $\langle p_T \rangle$ as function of multiplicity, the INEL data sample is subdivided into bins of n_{acc}. The results for $\langle p_T \rangle$ are presented calculating the weighted average over two different p_T ranges, $0.15 < p_T < 4$ GeV/c and $0.5 < p_T < 4$ GeV/c. In addition, results are presented employing the extrapolation to $p_T = 0$ as described above.

To extract the correlation between $\langle p_T \rangle$ and the number of primary charged particles (n_{ch}) in $|\eta| < 0.8$, the following weighting procedure is applied to account for the experimental resolution of the measured event multiplicities:

$$\langle p_T \rangle(n_{ch}) = \sum_{n_{acc}} \langle p_T \rangle(n_{acc}) R(n_{ch}, n_{acc}). \tag{3}$$

Table 1

Contributions to the systematic uncertainties on the differential primary charged particle yields $1/N_{\text{evt}}\,1/(2\pi p_T)\,\mathrm{d}^2 N_{\text{ch}}/(\mathrm{d}\eta\,\mathrm{d}p_T)$ and the average transverse momentum $\langle p_T \rangle$. Ranges are given if the contributions are p_T dependent.

p_T range (GeV/c)	$\frac{1}{N_{\text{evt}}}\frac{1}{2\pi p_T}\frac{\mathrm{d}^2 N_{\text{ch}}}{\mathrm{d}\eta\,\mathrm{d}p_T}$	$\langle p_T \rangle$		
	0.15–10	0.5–4	0.15–4	0–4 (extrap.)
Track selection cuts	0.2–4%	negl.	0.3%	0.5%
Contribution of diffraction (INEL)	0.9–1%	negl.	negl.	negl.
Contribution of diffraction (NSD)	2.8–3.9%	–	–	–
Event generator dependence (INEL)	2.5%	negl.	negl.	negl.
Event generator dependence (NSD)	0.5%	–	–	–
Particle composition	1–2%	0.1%	negl.	0.1%
Secondary particle rejection	0.2–1.5%	negl.	0.1%	0.2%
Detector misalignment	negl.	negl.	negl.	negl.
ITS efficiency	0–1.6%	negl.	0.3%	0.5%
TPC efficiency	0.8–4.5%	negl.	0.5%	0.7%
SPD triggering efficiency	negl.	negl.	negl.	negl.
VZERO triggering efficiency (INEL)	negl.	negl.	negl.	negl.
VZERO triggering efficiency (NSD)	0.2%	–	–	–
Beam-gas events	negl.	negl.	negl.	negl.
Pile-up events	negl.	negl.	negl.	negl.
Total (INEL)	3.0–7.1%	0.1%	0.7%	1.0%
Total (NSD)	3.5–7.2%	–	–	–
R weighting procedure		3.0%	3.0%	3.0%
Extrapolation to $p_T = 0$		–	–	1.0%
Total		3.0%	3.1%	3.3%

This method employs the normalized response matrix $R(n_{\text{ch}}, n_{\text{acc}})$ from Monte Carlo simulations which contains the probability that an event with multiplicity n_{ch} is reconstructed with multiplicity n_{acc}. The results from this approach are consistent with an alternative Monte Carlo based procedure, where an average multiplicity $\langle n_{\text{ch}} \rangle$ is assigned to every measured multiplicity n_{acc}.

4. Systematic uncertainties

In order to estimate the systematic uncertainties of the final p_T spectra, the results of the data analysis and of the evaluation of the corrections from Monte Carlo simulations are checked for stability under varying cuts and Monte Carlo assumptions, within reasonable limits. In particular we studied a variation of the ratios of the most abundant primary charged particles (p, π, K) by $\pm 30\%$ with respect to their PYTHIA values, the relative fractions of diffractive processes corresponding to their experimental errors [5,13], the TPC readout chamber alignment (± 100 μm), and track and event quality cuts in the analysis procedure. Particular attention was paid to the rejection efficiency of secondary particles using the d_0 cut. The stability of the results under variation of the d_0 cut value (± 3 standard deviations with respect to the nominal value), the secondary yield from strange hadron decays ($\pm 30\%$) and the material budget ($\pm 10\%$) was studied and the systematic uncertainty is estimated accordingly. Systematic uncertainties of the ITS and TPC detector efficiencies are estimated by a comparison of the experimental ITS–TPC track matching efficiency with the Monte Carlo one. The systematic uncertainty of the VZERO triggering efficiency is studied by varying the calibration and threshold settings in the data and in the Monte Carlo simulation. The event generator dependence is determined from a comparison of the PYTHIA results with those obtained using PHOJET. The total systematic uncertainty on the p_T spectra derived from this study is 3.0–7.1% for INEL events and 3.5–7.2% for NSD events, in the p_T range from 0.2–10 GeV/c (see Table 1).

Also listed in Table 1 are the systematic errors in $\langle p_T \rangle$ arising from these contributions. We note that only p_T dependent errors on the p_T spectra contribute to the systematic error in $\langle p_T \rangle$. Additional systematic uncertainties in $\langle p_T \rangle$ arise from the specific choice of the fit function used for the $p_T = 0$ extrapolation, and the weighting procedure which is employed to derive $\langle p_T \rangle$ as function of n_{ch}. To estimate the uncertainty in the extrapolation to $p_T = 0$ the results are compared to those obtained from a fit of the Tsallis function [17], or by fitting the spectral shape predicted by PYTHIA and PHOJET to our low p_T data points. Based on this comparison a systematic error of 1% in $\langle p_T \rangle$ is assigned to the $p_T = 0$ extrapolation. The weighting procedure (Eq. (3)) was studied using PYTHIA and PHOJET simulations. For both models, the true $\langle p_T \rangle$ dependence on n_{ch} from Monte Carlo can be recovered within 3% from the reconstructed dependence of $\langle p_T \rangle$ on n_{acc} using (3). No significant multiplicity dependence of the systematic errors on $\langle p_T \rangle$ is observed. The total systematic uncertainties on $\langle p_T \rangle$ are listed in Table 1.

5. Results and discussion

The normalized differential yield in INEL pp collisions at $\sqrt{s} = 900$ GeV and the fit with the parametrization given in Eq. (1) are shown in Fig. 2. The modified Hagedorn fit provides a good description of the data for $p_T < 4$ GeV/c. The fit parameters for INEL events are $p_{T,0} = 1.05 \pm 0.01$ (stat.) ± 0.05 (syst.) GeV/c and $b = 7.92 \pm 0.03$ (stat.) ± 0.02 (syst.). The average transverse momentum including the extrapolation to $p_T = 0$ is $\langle p_T \rangle_{\text{INEL}} = 0.483 \pm 0.001$ (stat.) ± 0.007 (syst.) GeV/c. For NSD events we obtain $p_{T,0} = 1.05 \pm 0.01$ (stat.) ± 0.05 (syst.) GeV/c, $b = 7.84 \pm 0.03$ (stat.) ± 0.02 (syst.) and $\langle p_T \rangle_{\text{NSD}} = 0.489 \pm 0.001$ (stat.) ± 0.007 (syst.) GeV/c. Restriction of the modified Hagedorn fit to $p_T < 4$ GeV/c has a negligible effect on these results. Fig. 2 also shows the result of a power law fit (Eq. (2)) to the INEL data for $p_T > 3$ GeV/c. The power law fit provides a significantly better description of the high p_T tail of the spectrum than the modified
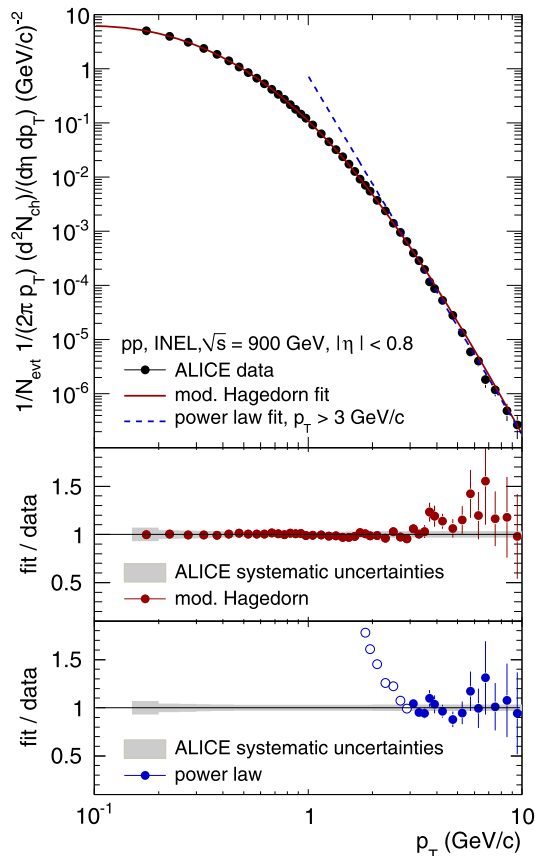
Fig. 2. Normalized differential primary charged particle yield in INEL pp collisions at $\sqrt{s} = 900$ GeV, averaged in $|\eta| < 0.8$. The fit ranges are $0.15 < p_T < 10$ GeV/c for the modified Hagedorn function (Eq. (1)) and $3 < p_T < 10$ GeV/c for the power law (Eq. (2)). In the lower panels, the ratios fit over data are shown. The open symbols indicate here data points which are not included in the fit. Errors bars are statistical only. Indicated as shaded areas are the relative systematic data errors.

Hagedorn parametrization. The result of the power law fit is $n = 6.63 \pm 0.12$ (stat.) ± 0.01 (syst.) for both INEL and NSD events. The power law shape of the high p_T part of the spectrum is suggestive of pQCD. Estimates of differential cross sections can be obtained using the cross sections derived from the measurement by UA5 [13] in $p\bar{p}$ at $\sqrt{s} = 900$ GeV, $\sigma_{\text{INEL}} = 50.3 \pm 0.4$ (stat.) ± 1 (syst.) mb and $\sigma_{\text{NSD}} = 42.6 \pm 1.4$ mb (see also [18]).

The transverse momentum distribution for NSD events is shown in Fig. 3 (left panel) together with data recently published by AT-LAS [19] and CMS [20], measured in larger pseudorapidity intervals. Below $p_T = 1$ GeV/c the data agree. At higher p_T the data are slightly above the other two LHC measurements. The observation of a harder spectrum is related to the different pseudorapidity windows (see below).

In the right panel of Fig. 3, the normalized invariant yield in NSD events is compared to measurements of the UA1 Collaboration in $p\bar{p}$ at the same energy [21], scaled by their measured NSD cross section of 43.5 mb. As in the previous comparison to ATLAS and CMS, the higher yield at large p_T may be related to the different pseudorapidity acceptances. The excess of the UA1 data of about 20% at low p_T is possibly due to the UA1 trigger condition, which suppresses events with very low multiplicity, as pointed out in [19].

The results for $\langle p_T \rangle$ in INEL and NSD events are compared to other experiments [20–25] in Fig. 4. Our results are somewhat higher than previous measurements in pp and $p\bar{p}$ at the same energy, but in larger pseudorapidity windows. This is consistent with the comparison of the spectra in Fig. 3. A similar trend exhibiting a larger $\langle p_T \rangle$ in a smaller pseudorapidity interval around mid-rapidity is apparent in Fig. 4 at Tevatron energies.

Indeed, a decrease of $\langle p_T \rangle$ by about 2% is found between $|\eta| < 0.2$ and $0.6 < |\eta| < 0.8$ in a pseudorapidity dependent analysis of the present data. A consistent decrease of $\langle p_T \rangle$ is also observed in the CMS data, when pseudorapidity is increased [20,26]. Likewise, a decrease of $\langle p_T \rangle$ by about 5% between $|\eta| < 0.8$ and $|\eta| < 2.5$ is found at $\sqrt{s} = 900$ GeV in PYTHIA.

Charged particle transverse momentum distributions can be used to tune Monte Carlo event generators of hadron–hadron interactions, such as PYTHIA and PHOJET. Recently, PYTHIA was tuned to describe the energy dependence of existing measurements, e.g. with respect to the treatment of multiple parton interactions and divergencies of the $2 \rightarrow 2$ parton scattering cross section at small momentum transfers.

In Fig. 5, the results for INEL events are compared to PHOJET and different tunes of PYTHIA, D6T (tune 109) [12], Perugia0 (tune 320) [27] and ATLAS-CSC (tune 306) [28]. The best agreement is found with the Perugia0 tune, which gives a fair description of the spectral shape, but is approximately 20% below the data. The D6T tune is similar to Perugia0 below 2 GeV/c but underestimates the data more significantly at high p_T. PHOJET and the PYTHIA ATLAS-CSC tune fail to reproduce the spectral shape of the data. They overestimate the yield below 0.7 GeV/c and fall short of the data at high p_T. We note that PHOJET and ATLAS-CSC agree best with the charged particle multiplicity distributions at $\sqrt{s} = 0.9$, 2.36 and 7 TeV, respectively [5,6].
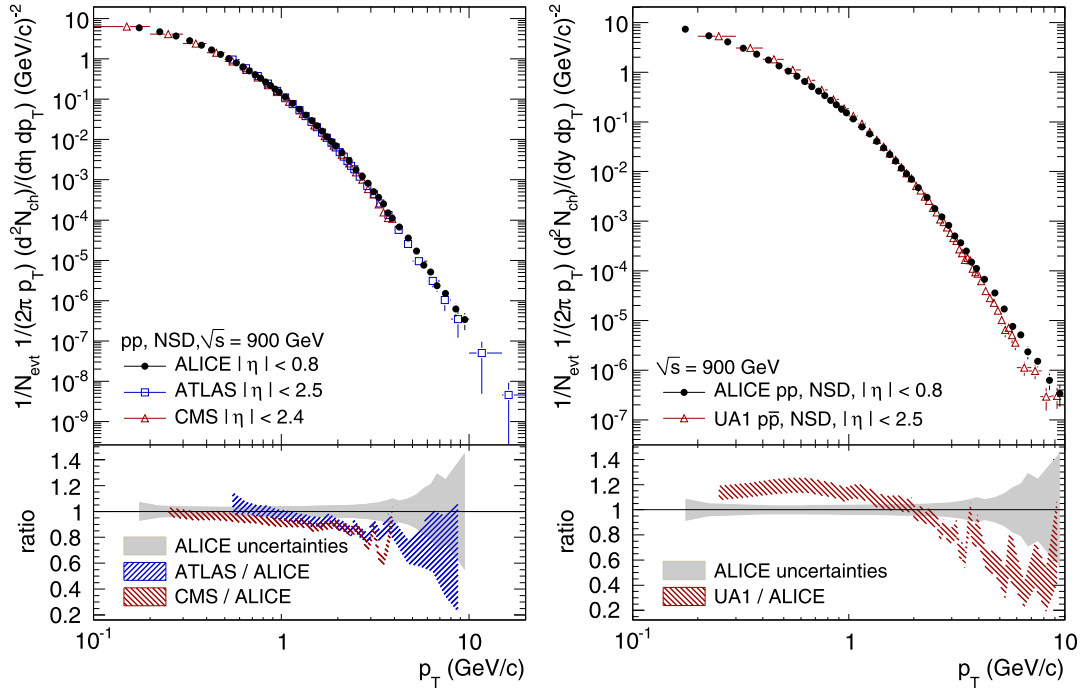
Fig. 3. Left panel: Normalized differential primary charged particle yield in NSD *pp* collisions at $\sqrt{s} = 900$ GeV, averaged in $|\eta| < 0.8$. The ALICE data are compared to results from ATLAS and CMS in *pp* at the same energy [19,20]. Right panel: Normalized invariant primary charged particle yield in NSD *pp* collisions at $\sqrt{s} = 900$ GeV, averaged in $|\eta| < 0.8$. The ALICE data are compared to results from UA1 in $p\bar{p}$ at the same energy [21]. For the computation of the invariant yield, it has been assumed that all particles are pions. The shaded areas indicate the statistical and systematic errors added in quadrature.
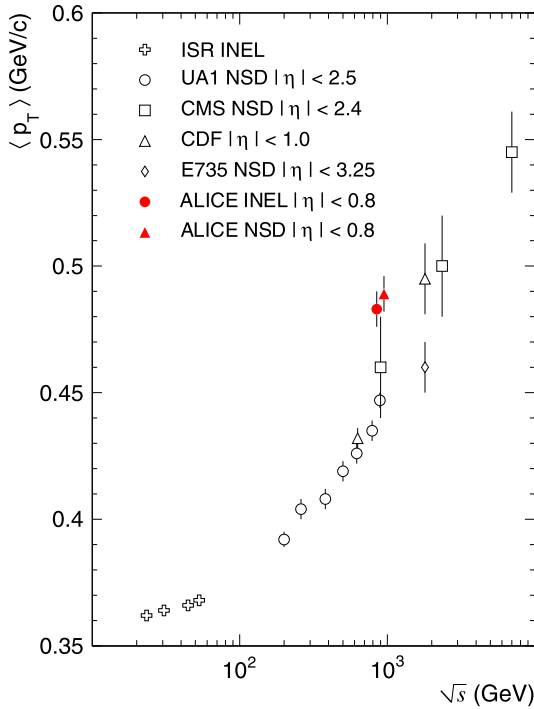
Fig. 4. Energy dependence of the average transverse momentum of primary charged particles in *pp* and $p\bar{p}$ collisions. Data from other experiments are taken from [20–25].
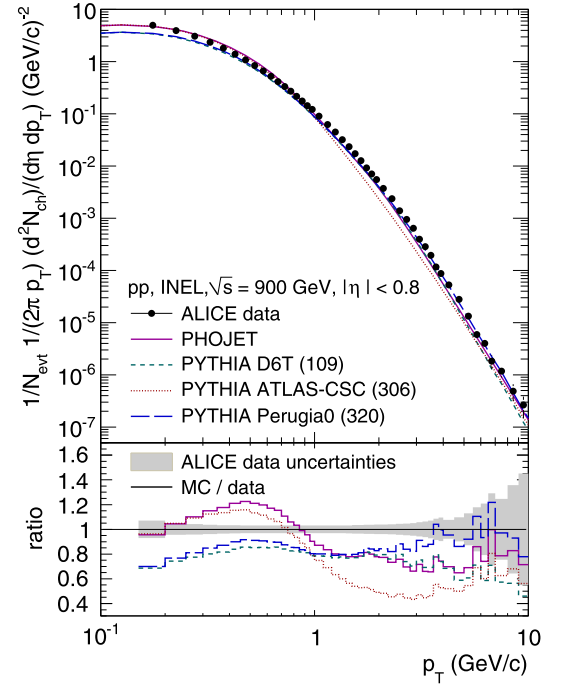
Fig. 5. Top: Comparison of the primary charged particle differential yield in INEL *pp* collisions at $\sqrt{s} = 900$ GeV ($|\eta| < 0.8$) to results from PHOJET and PYTHIA tunes 109 [12], 306 [28] and 320 [27]. Bottom: Ratio between the Monte Carlo simulation and the data. The shaded area indicates the statistical and systematic errors of the ALICE data added in quadrature.

Fig. 6 shows the p_T spectra in INEL events for three different multiplicity selections (n_{acc}) along with fits to the modified Hagedorn function (Eq. (1)). A considerable flattening of the tails of the spectra is visible with increasing multiplicity. The fit parameters $p_{T,0}$ and b drop by more than 50% from the lowest to the highest multiplicities. The results for the fit parameters in bins of n_{acc} are listed in Table 2, along with the average multiplicity $\langle n_{ch} \rangle$ assigned to each n_{acc} as determined from Monte Carlo simulations.
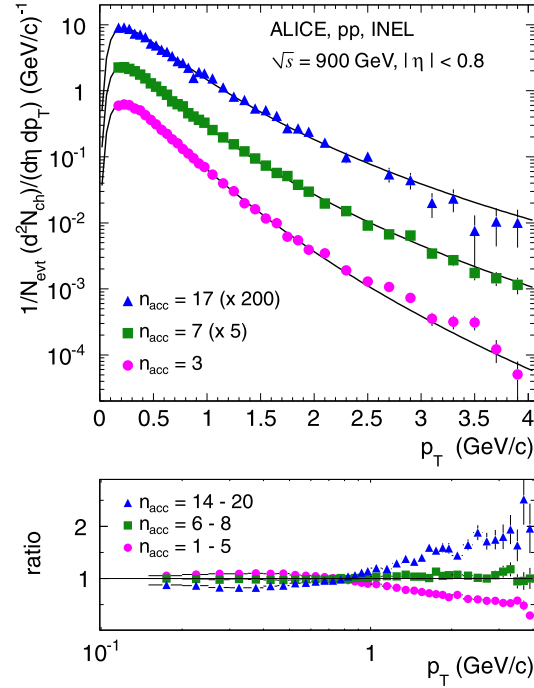
Fig. 6. Upper panel: Transverse momentum spectra of primary charged particles in INEL pp collisions at $\sqrt{s} = 900$ GeV ($|\eta| < 0.8$), normalized to the total number of INEL events N_{evt}, for three different event multiplicities together with the modified Hagedorn fits (Eq. (1)) described in the text. The fits are performed in the range $0.15 < p_T < 4$ GeV/c and extrapolated to $p_T = 0$. The error bars indicate the statistical and systematic errors added in quadrature. Lower panel: Ratios of the p_T spectra in different multiplicity ranges to the inclusive p_T spectrum in INEL events.

Table 2
Parameters of the modified Hagedorn fits (Eq. (1)) to the transverse momentum spectra. The fit range in p_T is 0.15–10 GeV/c for the multiplicity integrated spectra (first two rows) and 0.15–4 GeV/c for the spectra binned in multiplicity. The errors are statistical and systematic added in quadrature. Also given are the average multiplicities $\langle n_{ch} \rangle$ of events contributing to the n_{acc} bins, as determined from Monte Carlo.

Event class	n_{acc}	$\langle n_{ch} \rangle$	$p_{T,0}$ (GeV/c)	b
INEL	all		1.05 ± 0.05	7.92 ± 0.04
NSD	all		1.05 ± 0.05	7.84 ± 0.04
INEL	1	2.1 ± 0.1	2.64 ± 0.29	16.50 ± 1.32
INEL	2	3.5 ± 0.1	1.86 ± 0.15	12.58 ± 0.69
INEL	3	4.8 ± 0.1	1.49 ± 0.11	10.56 ± 0.45
INEL	4	6.1 ± 0.1	1.26 ± 0.08	9.28 ± 0.34
INEL	5	7.4 ± 0.1	1.16 ± 0.07	8.60 ± 0.28
INEL	6	8.7 ± 0.1	1.04 ± 0.06	7.87 ± 0.24
INEL	7	10.0 ± 0.2	1.01 ± 0.07	7.60 ± 0.23
INEL	8	11.3 ± 0.2	0.95 ± 0.05	7.27 ± 0.21
INEL	9	12.6 ± 0.2	0.97 ± 0.06	7.28 ± 0.22
INEL	10	13.9 ± 0.3	0.90 ± 0.06	6.87 ± 0.21
INEL	11	15.1 ± 0.3	0.91 ± 0.06	6.82 ± 0.21
INEL	12	16.4 ± 0.3	0.90 ± 0.06	6.80 ± 0.22
INEL	13	17.7 ± 0.4	0.91 ± 0.06	6.74 ± 0.23
INEL	14	18.9 ± 0.5	0.89 ± 0.06	6.65 ± 0.24
INEL	15	20.1 ± 0.5	0.96 ± 0.07	6.88 ± 0.27
INEL	16	21.3 ± 0.6	0.79 ± 0.06	6.14 ± 0.23
INEL	17	22.5 ± 0.5	0.92 ± 0.08	6.64 ± 0.30
INEL	18	23.7 ± 0.6	0.84 ± 0.08	6.29 ± 0.29
INEL	19	24.9 ± 0.7	0.80 ± 0.09	6.06 ± 0.31
INEL	20–21	26.6 ± 0.7	0.79 ± 0.09	6.03 ± 0.31
INEL	22–24	29.4 ± 0.8	0.78 ± 0.09	5.89 ± 0.32
INEL	25–27	33.0 ± 1.1	0.54 ± 0.10	5.02 ± 0.40
INEL	28–45	37.1 ± 1.5	0.59 ± 0.16	5.42 ± 0.67

Also shown in Fig. 6 are ratios of p_T spectra in different multiplicity regions over the inclusive p_T spectrum in INEL events. A very pronounced multiplicity dependence of the spectral shape is manifest, exhibiting enhanced particle production at high p_T in high multiplicity events. At $p_T < 0.8$ GeV/c the trend is opposite, albeit with a much weaker multiplicity dependence. The evolution of the spectral shape with multiplicity may shed light on different particle production mechanisms in pp collisions. A qualitatively similar evolution of the p_T spectra with multiplicity has been seen in pp data at $\sqrt{s} = 200$ GeV [29].
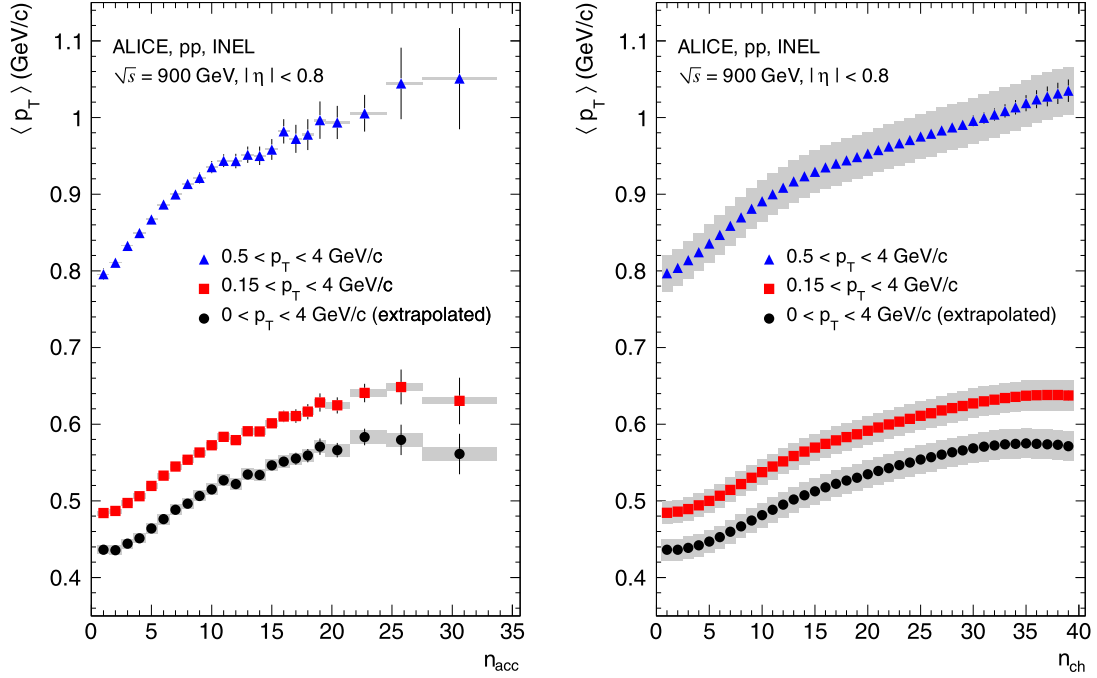
Fig. 7. The average transverse momentum of charged particles in INEL pp events at $\sqrt{s} = 900$ GeV for three different p_T ranges as a function of n_{acc} (left panel) and as a function of n_{ch} (right panel). The error bars and shaded areas indicate the statistical and systematic errors, respectively.
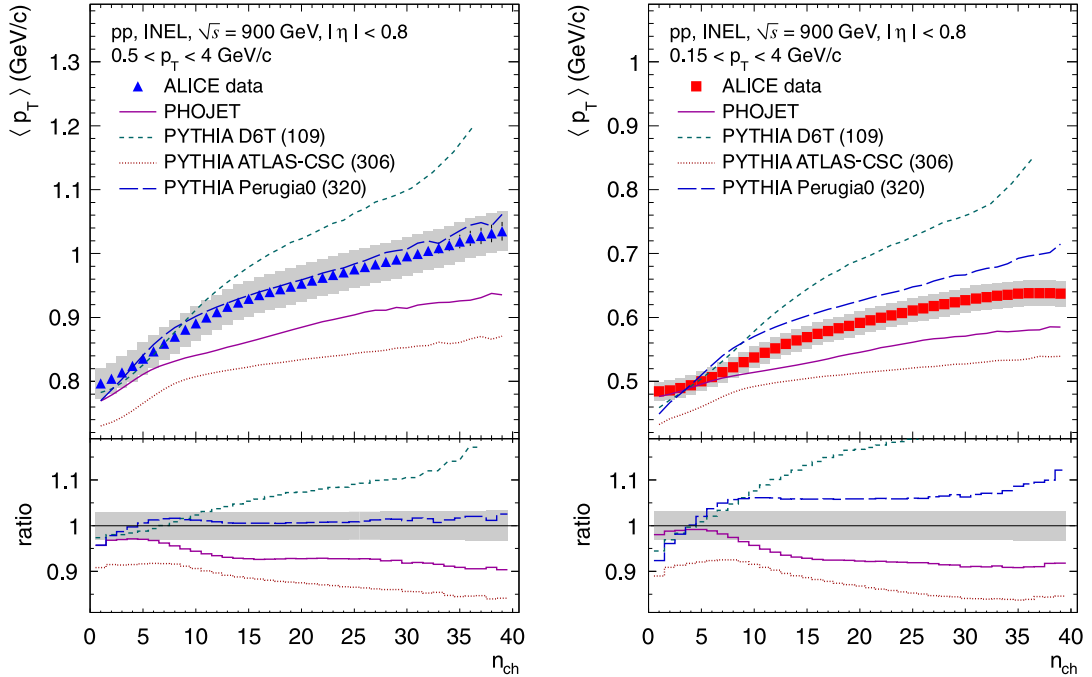
Fig. 8. The average transverse momentum of charged particles for $0.5 < p_T < 4$ GeV/c (left panel) and $0.15 < p_T < 4$ GeV/c (right panel) in INEL pp events at $\sqrt{s} = 900$ GeV as a function of n_{ch} in comparison to models. The error bars and the shaded area indicate the statistical and systematic errors of the data, respectively. In the lower panels, the ratio Monte Carlo over data is shown. The shaded areas indicate the statistical and systematic uncertainty of the data, added in quadrature.

The average transverse momentum $\langle p_T \rangle$ as a function of the multiplicity of accepted particles (n_{acc}) in INEL pp collisions at $\sqrt{s} = 900$ GeV is shown in the left panel of Fig. 7. For all three selected p_T ranges a significant increase of $\langle p_T \rangle$ with multiplicity is observed. Most significantly for $0.5 < p_T < 4$ GeV/c, the slope changes at intermediate multiplicities.

In the right panel of Fig. 7 the same data is shown as a function of n_{ch} after application of the weighting procedure (Eq. (3)). In comparison to model calculations, good agreement with the data for $0.5 < p_T < 4$ GeV/c is found only for the PYTHIA Perugia0 tune (Fig. 8, left panel). In a wider pseudorapidity interval ($|\eta| < 2.5$), similar agreement of the data with Perugia0 was reported by ATLAS [19]. For $0.15 < p_T < 4$ GeV/c, Perugia0 and PHOJET are the closest to the data, as shown in the right panel of Fig. 8, however, none of the models gives a good description of the entire measurements.

6. Conclusion

A measurement is presented of the primary charged particle transverse momentum spectrum and of the mean transverse momentum in pp collisions at $\sqrt{s} = 900$ GeV with the ALICE detector at the LHC. Good agreement with previous results from LHC is found up to $p_T = 1$ GeV/c. At higher p_T, the data exhibit a harder momentum spectrum of primary charged particles than other measurements in pp and $p\bar{p}$ collisions at the same energy. We argue that this is most likely related to the different pseudorapidity intervals studied. The average transverse momentum in $|\eta| < 0.8$ is $\langle p_T \rangle_{\text{INEL}} = 0.483 \pm 0.001$ (stat.) ± 0.007 (syst.) GeV/c and $\langle p_T \rangle_{\text{NSD}} = 0.489 \pm 0.001$ (stat.) ± 0.007 (syst.) GeV/c. None of the models and tunes investigated simultaneously describes the p_T spectrum and the correlation between $\langle p_T \rangle$ and n_{ch}. In particular in the low p_T region, where the bulk of the particles are produced, the models require further tuning. These measurements will help to improve the phenomenological description of soft QCD processes and the interplay between soft and hard QCD. The presented data demonstrate the excellent performance of the ALICE detector for momentum measurement and will be used as a baseline for measurements at higher LHC energies and for comparison with particle production in heavy-ion collisions.

References

[1] L. Evans, P. Bryant (Eds.), JINST 3 (2008) S08001.
[2] T. Sjöstrand, S. Mrenna, P. Skands, J. High Energy Phys. 0605 (2006) 026.
[3] R. Engel, J. Ranft, S. Roesler, Phys. Rev. D 52 (1995) 1459.
[4] ALICE Collaboration, K. Aamodt, et al., Eur. Phys. J. C 65 (2010) 111, arXiv:0911.5430 [hep-ex].
[5] ALICE Collaboration, K. Aamodt, et al., Eur. Phys. J. C 68 (2010) 89, arXiv:1004.3034 [hep-ex].

[6] ALICE Collaboration, K. Aamodt, et al., Eur. Phys. J. C 68 (2010) 345, arXiv:1004.3514 [hep-ex].
[7] ALICE Collaboration, J. Phys. G 30 (2004) 1517;
ALICE Collaboration, J. Phys. G 32 (2006) 1295.
[8] ALICE Collaboration, K. Aamodt, et al., JINST 3 (2008) S08002.
[9] ALICE Collaboration, J. Alme, et al., Nucl. Instrum. Methods A 622 (2010) 316, arXiv:1001.1950 [physics.ins-det].
[10] ALICE Collaboration, K. Aamodt, et al., JINST 5 (2010) P03003.
[11] ALICE Collaboration, R. Brun, et al., Nucl. Instrum. Methods A 502 (2003) 339.
[12] M. Albrow, et al., Tevatron-for-LHC Conference Report of the QCD Working Group, Fermilab-Conf-06-359, hep-ph/0610012;
T. Sjöstrand, P. Skands, Eur. Phys. J. C 39 (2005) 129.
[13] UA5 Collaboration, R.E. Ansorge, et al., Z. Phys. C 33 (1986) 175.
[14] H. Ricaud, A. Kalweit, A. Maire, for the ALICE Collaboration, J. Phys. G 37 (2010) 094049, arXiv:1003.4609.
[15] STAR Collaboration, B.I. Abelev, et al., Phys. Rev. C 75 (2007) 064901.
[16] R. Hagedorn, Riv. Nuovo Cimento 6 (1983) 1.
[17] C. Tsallis, J. Stat. Phys. 52 (1988) 479.
[18] M.G. Poghosyan, arXiv:1005.1806 [hep-ph].
[19] ATLAS Collaboration, G. Aad, et al., Phys. Lett. B 688 (2010) 121, arXiv:1003.3124 [hep-ex].
[20] CMS Collaboration, V. Khachatryan, et al., JHEP 1002 (2010) 041.
[21] UA1 Collaboration, C. Albajar, et al., Nucl. Phys. B 335 (1990) 261.
[22] A.M. Rossi, G. Vannini, A. Bussiere, E. Albini, D. D'Alessandro, G. Giacomelli, Nucl. Phys. B 84 (1975) 269.
[23] E735 Collaboration, T. Alexopoulos, et al., Phys. Rev. Lett. 60 (1988) 1622.
[24] CDF Collaboration, F. Abe, et al., Phys. Rev. Lett. 61 (1988) 1819.
[25] CMS Collaboration, V. Khachatryan, et al., Phys. Rev. Lett. 105 (2010) 022002, arXiv:1005.3299 [hep-ex].
[26] CMS Collaboration, http://cdsweb.cern.ch/record/1237408/files/~13130_2010_170_MOESM1_ESM.txt.
[27] P. Skands, Contribution to the 1st International Workshop on Multiple Partonic Interactions at the LHC, Perugia, Italy, Oct. 2008, Fermilab-Conf-09-113-T, arXiv:0905.3418 [hep-ph].
[28] ATLAS Collaboration, A. Moraes, ATLAS Note ATL-COM-PHYS-2009-119 (2009).
[29] Z. Chajecki, M. Lisa, Phys. Rev. C 79 (2009) 034908.

ALICE Collaboration

K. Aamodt [by], N. Abel [aq], U. Abeysekara [bw], A. Abrahantes Quintana [ap], A. Abramyan [dh], D. Adamová [cg], M.M. Aggarwal [y], G. Aglieri Rinella [an], A.G. Agocs [r], S. Aguilar Salazar [bk], Z. Ahammed [ba], A. Ahmad [b], N. Ahmad [b], S.U. Ahn [al,1], R. Akimoto [cu], A. Akindinov [bn], D. Aleksandrov [bp], B. Alessandro [cz], R. Alfaro Molina [bk], A. Alici [m], E. Almaráz Aviña [bk], J. Alme [h], T. Alt [aq,2], V. Altini [e], S. Altinpinar [ae], C. Andrei [q], A. Andronic [ae], G. Anelli [an], V. Angelov [aq,2], C. Anson [aa], T. Antičić [di], F. Antinori [an,3], S. Antinori [m], K. Antipin [aj], D. Antończyk [aj], P. Antonioli [n], A. Anzo [bk], L. Aphecetche [bs], H. Appelshäuser [aj,*], S. Arcelli [m], R. Arceo [bk], A. Arend [aj], N. Armesto [cm], R. Arnaldi [cz], T. Aronsson [bt], I.C. Arsene [by,4], A. Asryan [cs], A. Augustinus [an], R. Averbeck [ae], T.C. Awes [bv], J. Äystö [aw], M.D. Azmi [b], S. Bablok [h], M. Bach [ai], A. Badalà [x], Y.W. Baek [al,1], S. Bagnasco [cz], R. Bailhache [ae,5], R. Bala [cy], A. Baldisseri [cj], A. Baldit [z], J. Bán [bd], R. Barbera [w], G.G. Barnaföldi [r], L. Barnby [l], V. Barret [z], J. Bartke [ac], F. Barile [e], M. Basile [m], V. Basmanov [co], N. Bastid [z], B. Bathen [br], G. Batigne [bs], B. Batyunya [ah], C. Baumann [br,5], I.G. Bearden [ab], B. Becker [t,6], I. Belikov [ct], R. Bellwied [ag], E. Belmont-Moreno [bk], A. Belogianni [d], L. Benhabib [bs], S. Beole [cy], I. Berceanu [q], A. Bercuci [ae,7], E. Berdermann [ae], Y. Berdnikov [am], L. Betev [an], A. Bhasin [av], A.K. Bhati [y], L. Bianchi [cy], N. Bianchi [ak], C. Bianchin [bz], J. Bielčík [cb], J. Bielčíková [cg], A. Bilandzic [c], L. Bimbot [bx], E. Biolcati [cy], A. Blanc [z], F. Blanco [w,8], F. Blanco [bi], D. Blau [bp], C. Blume [aj], M. Boccioli [an], N. Bock [aa], A. Bogdanov [bo], H. Bøggild [ab], M. Bogolyubsky [cd], J. Bohm [cq], L. Boldizsár [r], M. Bombara [bc], C. Bombonati [bz,10], M. Bondila [aw], H. Borel [cj], A. Borisov [ax], C. Bortolin [bz,34], S. Bose [az], L. Bosisio [cv], F. Bossú [cy], M. Botje [c], S. Böttger [aq], G. Bourdaud [bs], B. Boyer [bx], M. Braun [cs], P. Braun-Munzinger [ae,af,2], L. Bravina [by], M. Bregant [cv,11], T. Breitner [aq], G. Bruckner [an], R. Brun [an], E. Bruna [bt], G.E. Bruno [e], D. Budnikov [co], H. Buesching [aj], P. Buncic [an], O. Busch [ar], Z. Buthelezi [v], D. Caffarri [bz], X. Cai [dg], H. Caines [bt], E. Calvo [bf], E. Camacho [bl], P. Camerini [cv], M. Campbell [an], V. Canoa Roman [an], G.P. Capitani [ak], G. Cara Romeo [n], F. Carena [an], W. Carena [an], F. Carminati [an], A. Casanova Díaz [ak], M. Caselle [an], J. Castillo Castellanos [cj], J.F. Castillo Hernandez [ae], V. Catanescu [q], E. Cattaruzza [cv], C. Cavicchioli [an], P. Cerello [cz], V. Chambert [bx], B. Chang [cq], S. Chapeland [an], A. Charpy [bx], J.L. Charvet [cj], S. Chattopadhyay [az], S. Chattopadhyay [ba], M. Cherney [bw], C. Cheshkov [an], B. Cheynis [db], E. Chiavassa [cy], V. Chibante Barroso [an], D.D. Chinellato [u], P. Chochula [an], K. Choi [cf], M. Chojnacki [da], P. Christakoglou [da], C.H. Christensen [ab], P. Christiansen [bh], T. Chujo [cx], F. Chuman [as], C. Cicalo [t], L. Cifarelli [m], F. Cindolo [n], J. Cleymans [v], O. Cobanoglu [cy], J.-P. Coffin [ct], S. Coli [cz], A. Colla [an], G. Conesa Balbastre [ak], Z. Conesa del Valle [bs,12], E.S. Conner [df], P. Constantin [ar], G. Contin [cv,10], J.G. Contreras [bl], Y. Corrales Morales [cy], T.M. Cormier [ag], P. Cortese [a], I. Cortés Maldonado [ce], M.R. Cosentino [u], F. Costa [an], M.E. Cotallo [bi], E. Crescio [bl], P. Crochet [z], E. Cuautle [bj], L. Cunqueiro [ak],

J. Cussonneau [bs], A. Dainese [ca], H.H. Dalsgaard [ab], A. Danu [p], I. Das [az], A. Dash [k], S. Dash [k],
G.O.V. de Barros [cn], A. De Caro [ck], G. de Cataldo [f], J. de Cuveland [aq,2], A. De Falco [s], M. De Gaspari [ar],
J. de Groot [an], D. De Gruttola [ck], N. De Marco [cz], S. De Pasquale [ck], R. De Remigis [cz], R. de Rooij [da],
G. de Vaux [v], H. Delagrange [bs], Y. Delgado [bf], G. Dellacasa [a], A. Deloff [dc], V. Demanov [co], E. Dénes [r],
A. Deppman [cn], G. D'Erasmo [e], D. Derkach [cs], A. Devaux [z], D. Di Bari [e], C. Di Giglio [e,10], S. Di Liberto [ci],
A. Di Mauro [an], P. Di Nezza [ak], M. Dialinas [bs], L. Díaz [bj], R. Díaz [aw], T. Dietel [br], R. Divià [an], Ø. Djuvsland [h],
V. Dobretsov [bp], A. Dobrin [bh], T. Dobrowolski [dc], B. Dönigus [ae], I. Domínguez [bj], D.M.M. Don [at],
O. Dordic [by], A.K. Dubey [ba], J. Dubuisson [an], L. Ducroux [db], P. Dupieux [z], A.K. Dutta Majumdar [az],
M.R. Dutta Majumdar [ba], D. Elia [f], D. Emschermann [ar,13], A. Enokizono [bv], B. Espagnon [bx], M. Estienne [bs],
S. Esumi [cx], D. Evans [l], S. Evrard [an], G. Eyyubova [by], C.W. Fabjan [an,14], D. Fabris [ca], J. Faivre [ao],
D. Falchieri [m], A. Fantoni [ak], M. Fasel [ae], O. Fateev [ah], R. Fearick [v], A. Fedunov [ah], D. Fehlker [h], V. Fekete [o],
D. Felea [p], B. Fenton-Olsen [ab,15], G. Feofilov [cs], A. Fernández Téllez [ce], E.G. Ferreiro [cm], A. Ferretti [cy],
R. Ferretti [a,16], M.A.S. Figueredo [cn], S. Filchagin [co], R. Fini [f], F.M. Fionda [e], E.M. Fiore [e], M. Floris [s,10],
Z. Fodor [r], S. Foertsch [v], P. Foka [ae], S. Fokin [bp], F. Formenti [an], E. Fragiacomo [cw], M. Fragkiadakis [d],
U. Frankenfeld [ae], A. Frolov [bu], U. Fuchs [an], F. Furano [an], C. Furget [ao], M. Fusco Girard [ck], J.J. Gaardhøje [ab],
S. Gadrat [ao], M. Gagliardi [cy], A. Gago [bf], M. Gallio [cy], P. Ganoti [d], M.S. Ganti [ba], C. Garabatos [ae],
C. García Trapaga [cy], J. Gebelein [aq], R. Gemme [a], M. Germain [bs], A. Gheata [an], M. Gheata [an], B. Ghidini [e],
P. Ghosh [ba], G. Giraudo [cz], P. Giubellino [cz], E. Gladysz-Dziadus [ac], R. Glasow [br,17], P. Glässel [ar], A. Glenn [bg],
R. Gómez Jiménez [ad], H. González Santos [ce], L.H. González-Trueba [bk], P. González-Zamora [bi],
S. Gorbunov [aq,2], Y. Gorbunov [bw], S. Gotovac [cr], H. Gottschlag [br], V. Grabski [bk], R. Grajcarek [ar], A. Grelli [da],
A. Grigoras [an], C. Grigoras [an], V. Grigoriev [bo], A. Grigoryan [dh], S. Grigoryan [ah], B. Grinyov [ax], N. Grion [cw],
P. Gros [bh], J.F. Grosse-Oetringhaus [an], J.-Y. Grossiord [db], R. Grosso [ca], F. Guber [bm], R. Guernane [ao],
C. Guerra [bf], B. Guerzoni [m], K. Gulbrandsen [ab], H. Gulkanyan [dh], T. Gunji [cu], A. Gupta [av], R. Gupta [av],
H.-A. Gustafsson [bh,17], H. Gutbrod [ae], Ø. Haaland [h], C. Hadjidakis [bx], M. Haiduc [p], H. Hamagaki [cu],
G. Hamar [r], J. Hamblen [ay], B.H. Han [cp], J.W. Harris [bt], M. Hartig [aj], A. Harutyunyan [dh], D. Hasch [ak],
D. Hasegan [p], D. Hatzifotiadou [n], A. Hayrapetyan [dh], M. Heide [br], M. Heinz [bt], H. Helstrup [i],
A. Herghelegiu [q], C. Hernández [ae], G. Herrera Corral [bl], N. Herrmann [ar], K.F. Hetland [i], B. Hicks [bt],
A. Hiei [as], P.T. Hille [by,18], B. Hippolyte [ct], T. Horaguchi [as,19], Y. Hori [cu], P. Hristov [an], I. Hřivnáčová [bx],
S. Hu [g], M. Huang [h], S. Huber [ae], T.J. Humanic [aa], D. Hutter [ai], D.S. Hwang [cp], R. Ichou [bs], R. Ilkaev [co],
I. Ilkiv [dc], M. Inaba [cx], P.G. Innocenti [an], M. Ippolitov [bp], M. Irfan [b], C. Ivan [da], A. Ivanov [cs], M. Ivanov [ae],
V. Ivanov [am], T. Iwasaki [as], A. Jachołkowski [an], P. Jacobs [j], L. Jančurová [ah], S. Jangal [ct], R. Janik [o], C. Jena [k],
S. Jena [bq], L. Jirden [an], G.T. Jones [l], P.G. Jones [l], P. Jovanović [l], H. Jung [al], W. Jung [al], A. Jusko [l],
A.B. Kaidalov [bn], S. Kalcher [aq,2], P. Kaliňák [bd], M. Kalisky [br], T. Kalliokoski [aw], A. Kalweit [af], A. Kamal [b],
R. Kamermans [da], K. Kanaki [h], E. Kang [al], J.H. Kang [cq], J. Kapitan [cg], V. Kaplin [bo], S. Kapusta [an],
O. Karavichev [bm], T. Karavicheva [bm], E. Karpechev [bm], A. Kazantsev [bp], U. Kebschull [aq], R. Keidel [df],
M.M. Khan [b], S.A. Khan [ba], A. Khanzadeev [am], Y. Kharlov [cd], D. Kikola [dd], B. Kileng [i], D.J. Kim [aw], D.S. Kim [al],
D.W. Kim [al], H.N. Kim [al], J. Kim [cd], J.H. Kim [cp], J.S. Kim [al], M. Kim [al], M. Kim [cq], S.H. Kim [al], S. Kim [cp],
Y. Kim [cq], S. Kirsch [an], I. Kisel [aq,4], S. Kiselev [bn], A. Kisiel [aa,10], J.L. Klay [cl], J. Klein [ar], C. Klein-Bösing [an,13],
M. Kliemant [aj], A. Klovning [h], A. Kluge [an], M.L. Knichel [ae], S. Kniege [aj], K. Koch [ar], R. Kolevatov [by],
A. Kolojvari [cs], V. Kondratiev [cs], N. Kondratyeva [bo], A. Konevskih [bm], E. Kornaś [ac], R. Kour [l], M. Kowalski [ac],
S. Kox [ao], K. Kozlov [bp], J. Kral [cb,11], I. Králik [bd], F. Kramer [aj], I. Kraus [af,4], A. Kravčáková [bc],
T. Krawutschke [bb], M. Krivda [l], D. Krumbhorn [ar], M. Krus [cb], E. Kryshen [am], M. Krzewicki [c],
Y. Kucheriaev [bp], C. Kuhn [ct], P.G. Kuijer [c], L. Kumar [y], N. Kumar [y], R. Kupczak [dd], P. Kurashvili [dc],
A. Kurepin [bm], A.N. Kurepin [bm], A. Kuryakin [co], S. Kushpil [cg], V. Kushpil [cg], M. Kutouski [ah], H. Kvaerno [by],
M.J. Kweon [ar], Y. Kwon [cq], P. La Rocca [w,20], F. Lackner [an], P. Ladrón de Guevara [bi], V. Lafage [bx], C. Lal [av],
C. Lara [aq], D.T. Larsen [h], G. Laurenti [n], C. Lazzeroni [l], Y. Le Bornec [bx], N. Le Bris [bs], H. Lee [cf], K.S. Lee [al],
S.C. Lee [al], F. Lefèvre [bs], M. Lenhardt [bs], L. Leistam [an], J. Lehnert [aj], V. Lenti [f], H. León [bk], I. León Monzón [ad],
H. León Vargas [aj], P. Lévai [r], X. Li [g], Y. Li [g], R. Lietava [l], S. Lindal [by], V. Lindenstruth [aq,2], C. Lippmann [an],
M.A. Lisa [aa], L. Liu [h], V. Loginov [bo], S. Lohn [an], X. Lopez [z], M. López Noriega [bx], R. López-Ramírez [ce],
E. López Torres [ap], G. Løvhøiden [by], A. Lozea Feijo Soares [cn], S. Lu [g], P. Luettig [aj], M. Lunardon [bz],
G. Luparello [cy], L. Luquin [bs], J.-R. Lutz [ct], K. Ma [dg], R. Ma [bt], D.M. Madagodahettige-Don [at],
A. Maevskaya [bm], M. Mager [af,10], D.P. Mahapatra [k], A. Maire [ct], I. Makhlyueva [an], D. Mal'Kevich [bn],

M. Malaev [am], K.J. Malagalage [bw], I. Maldonado Cervantes [bj], M. Malek [bx], T. Malkiewicz [aw],
P. Malzacher [ae], A. Mamonov [co], L. Manceau [z], L. Mangotra [av], V. Manko [bp], F. Manso [z], V. Manzari [f],
Y. Mao [dg,21], J. Mareš [cc], G.V. Margagliotti [cv], A. Margotti [n], A. Marín [ae], I. Martashvili [ay], P. Martinengo [an],
M.I. Martínez Hernández [ce], A. Martínez Davalos [bk], G. Martínez García [bs], Y. Maruyama [as],
A. Marzari Chiesa [cy], S. Masciocchi [ae], M. Masera [cy], M. Masetti [m], A. Masoni [t], L. Massacrier [db],
M. Mastromarco [f], A. Mastroserio [e,10], Z.L. Matthews [l], A. Matyja [ac,29], D. Mayani [bj], G. Mazza [cz],
M.A. Mazzoni [ci], F. Meddi [ch], A. Menchaca-Rocha [bk], P. Mendez Lorenzo [an], M. Meoni [an],
J. Mercado Pérez [ar], P. Mereu [cz], Y. Miake [cx], A. Michalon [ct], N. Miftakhov [am], L. Milano [cy], J. Milosevic [by],
F. Minafra [e], A. Mischke [da], D. Miśkowiec [ae], C. Mitu [p], K. Mizoguchi [as], J. Mlynarz [ag], B. Mohanty [ba],
L. Molnar [r,10], M.M. Mondal [ba], L. Montaño Zetina [bl,22], M. Monteno [cz], E. Montes [bi], M. Morando [bz],
S. Moretto [bz], A. Morsch [an], T. Moukhanova [bp], V. Muccifora [ak], E. Mudnic [cr], S. Muhuri [ba], H. Müller [an],
M.G. Munhoz [cn], J. Munoz [ce], L. Musa [an], A. Musso [cz], B.K. Nandi [bq], R. Nania [n], E. Nappi [f], F. Navach [e],
S. Navin [l], T.K. Nayak [ba], S. Nazarenko [co], G. Nazarov [co], A. Nedosekin [bn], F. Nendaz [db], J. Newby [bg],
A. Nianine [bp], M. Nicassio [f,10], B.S. Nielsen [ab], S. Nikolaev [bp], V. Nikolic [di], S. Nikulin [bp], V. Nikulin [am],
B.S. Nilsen [bw], M.S. Nilsson [by], F. Noferini [n], P. Nomokonov [ah], G. Nooren [da], N. Novitzky [aw], A. Nyatha [bq],
C. Nygaard [ab], A. Nyiri [by], J. Nystrand [h], A. Ochirov [cs], G. Odyniec [j], H. Oeschler [af], M. Oinonen [aw],
K. Okada [cu], Y. Okada [as], M. Oldenburg [an], J. Oleniacz [dd], C. Oppedisano [cz], F. Orsini [cj], A. Ortiz Velasquez [bj],
G. Ortona [cy], A. Oskarsson [bh], F. Osmic [an], L. Österman [bh], P. Ostrowski [dd], I. Otterlund [bh], J. Otwinowski [ae],
G. Øvrebekk [h], K. Oyama [ar], K. Ozawa [cu], Y. Pachmayer [ar], M. Pachr [cb], F. Padilla [cy], P. Pagano [ck],
G. Paić [bj], F. Painke [aq], C. Pajares [cm], S. Pal [az,23], S.K. Pal [ba], A. Palaha [l], A. Palmeri [x], R. Panse [aq],
V. Papikyan [dh], G.S. Pappalardo [x], W.J. Park [ae], B. Pastirčák [bd], C. Pastore [f], V. Paticchio [f], A. Pavlinov [ag],
T. Pawlak [dd], T. Peitzmann [da], A. Pepato [ca], H. Pereira [cj], D. Peressounko [bp], C. Pérez [bf], D. Perini [an],
D. Perrino [e,10], W. Peryt [dd], J. Peschek [aq,2], A. Pesci [n], V. Peskov [bj,10], Y. Pestov [bu], A.J. Peters [an],
V. Petráček [cb], A. Petridis [d,17], M. Petris [q], P. Petrov [l], M. Petrovici [q], C. Petta [w], J. Peyré [bx], S. Piano [cw],
A. Piccotti [cz], M. Pikna [o], P. Pillot [bs], O. Pinazza [n,10], L. Pinsky [at], N. Pitz [aj], F. Piuz [an], R. Platt [l], M. Płoskoń [j],
J. Pluta [dd], T. Pocheptsov [ah,24], S. Pochybova [r], P.L.M. Podesta Lerma [ad], F. Poggio [cy], M.G. Poghosyan [cy],
K. Polák [cc], B. Polichtchouk [cd], P. Polozov [bn], V. Polyakov [am], B. Pommeresch [h], A. Pop [q], F. Posa [e],
V. Pospíšil [cb], B. Potukuchi [av], J. Pouthas [bx], S.K. Prasad [ba], R. Preghenella [m,20], F. Prino [cz], C.A. Pruneau [ag],
I. Pshenichnov [bm], G. Puddu [s], P. Pujahari [bq], A. Pulvirenti [w], A. Punin [co], V. Punin [co], M. Putiš [bc],
J. Putschke [bt], E. Quercigh [an], A. Rachevski [cw], A. Rademakers [an], S. Radomski [ar], T.S. Räihä [aw], J. Rak [aw],
A. Rakotozafindrabe [cj], L. Ramello [a], A. Ramírez Reyes [bl], M. Rammler [br], R. Raniwala [au], S. Raniwala [au],
S.S. Räsänen [aw], I. Rashevskaya [cw], S. Rath [k], K.F. Read [ay], J.S. Real [ao], K. Redlich [dc,35], R. Renfordt [aj],
A.R. Reolon [ak], A. Reshetin [bm], F. Rettig [aq,2], J.-P. Revol [an], K. Reygers [br,25], H. Ricaud [af], L. Riccati [cz],
R.A. Ricci [be], M. Richter [h], P. Riedler [an], W. Riegler [an], F. Riggi [w], A. Rivetti [cz], M. Rodriguez Cahuantzi [ce],
K. Røed [i], D. Röhrich [an,26], S. Román López [ce], R. Romita [e,4], F. Ronchetti [ak], P. Rosinský [an],
P. Rosnet [z], S. Rossegger [an], A. Rossi [cv,36], F. Roukoutakis [an,27], S. Rousseau [bx], C. Roy [bs,12],
P. Roy [az], A.J. Rubio-Montero [bi], R. Rui [cv], I. Rusanov [ar], G. Russo [ck], E. Ryabinkin [bp], A. Rybicki [ac],
S. Sadovsky [cd], K. Šafařík [an], R. Sahoo [bz], J. Saini [ba], P. Saiz [an], D. Sakata [cx], C.A. Salgado [cm],
R. Salgueiro Domingues da Silva [an], S. Salur [j], T. Samanta [ba], S. Sambyal [av], V. Samsonov [am], L. Šándor [bd],
A. Sandoval [bk], M. Sano [cx], S. Sano [cu], R. Santo [br], R. Santoro [e], J. Sarkamo [aw], P. Saturnini [z],
E. Scapparone [n], F. Scarlassara [bz], R.P. Scharenberg [de], C. Schiaua [q], R. Schicker [ar], H. Schindler [an],
C. Schmidt [ae], H.R. Schmidt [ae], K. Schossmaier [an], S. Schreiner [an], S. Schuchmann [aj], J. Schukraft [an],
Y. Schutz [bs], K. Schwarz [ae], K. Schweda [ar], G. Scioli [m], E. Scomparin [cz], P.A. Scott [l], G. Segato [bz],
D. Semenov [cs], S. Senyukov [a], J. Seo [al], S. Serci [s], L. Serkin [bj], E. Serradilla [bi], A. Sevcenco [p], I. Sgura [e],
G. Shabratova [ah], R. Shahoyan [an], G. Sharkov [bn], N. Sharma [y], S. Sharma [av], K. Shigaki [as], M. Shimomura [cx],
K. Shtejer [ap], Y. Sibiriak [bp], M. Siciliano [cy], E. Sicking [an,28], E. Siddi [t], T. Siemiarczuk [dc], A. Silenzi [m],
D. Silvermyr [bv], E. Simili [da], G. Simonetti [e,10], R. Singaraju [ba], R. Singh [av], V. Singhal [ba], B.C. Sinha [ba],
T. Sinha [az], B. Sitar [o], M. Sitta [a], T.B. Skaali [by], K. Skjerdal [h], R. Smakal [cb], N. Smirnov [bt], R. Snellings [c],
H. Snow [l], C. Søgaard [ab], A. Soloviev [cd], H.K. Soltveit [ar], R. Soltz [bg], W. Sommer [aj], C.W. Son [cf], H. Son [cp],
M. Song [cq], C. Soos [an], F. Soramel [bz], D. Soyk [ae], M. Spyropoulou-Stassinaki [d], B.K. Srivastava [de], J. Stachel [ar],
F. Staley [cj], E. Stan [p], G. Stefanek [dc], G. Stefanini [an], T. Steinbeck [aq,2], E. Stenlund [bh], G. Steyn [v],
D. Stocco [cy,29], R. Stock [aj], P. Stolpovsky [cd], P. Strmen [o], A.A.P. Suaide [cn], M.A. Subieta Vásquez [cy],

T. Sugitate [as], C. Suire [bx], M. Šumbera [cg], T. Susa [di], D. Swoboda [an], J. Symons [j], A. Szanto de Toledo [cn], I. Szarka [o], A. Szostak [t], M. Szuba [dd], M. Tadel [an], C. Tagridis [d], A. Takahara [cu], J. Takahashi [u], R. Tanabe [cx], J.D. Tapia Takaki [bx], H. Taureg [an], A. Tauro [an], M. Tavlet [an], G. Tejeda Muñoz [ce], A. Telesca [an], C. Terrevoli [e], J. Thäder [aq,2], R. Tieulent [db], D. Tlusty [cb], A. Toia [an], T. Tolyhy [r], C. Torcato de Matos [an], H. Torii [as], G. Torralba [aq], L. Toscano [cz], F. Tosello [cz], A. Tournaire [bs,30], T. Traczyk [dd], P. Tribedy [ba], G. Tröger [aq], D. Truesdale [aa], W.H. Trzaska [aw], G. Tsiledakis [ar], E. Tsilis [d], T. Tsuji [cu], A. Tumkin [co], R. Turrisi [ca], A. Turvey [bw], T.S. Tveter [by], H. Tydesjö [an], K. Tywoniuk [by], J. Ulery [aj], K. Ullaland [h], A. Uras [s], J. Urbán [bc], G.M. Urciuoli [ci], G.L. Usai [s], A. Vacchi [cw], M. Vala [ah,9], L. Valencia Palomo [bk], S. Vallero [ar], N. van der Kolk [c], P. Vande Vyvre [an], M. van Leeuwen [da], L. Vannucci [be], A. Vargas [ce], R. Varma [bq], A. Vasiliev [bp], I. Vassiliev [aq,27], M. Vasileiou [d], V. Vechernin [cs], M. Venaruzzo [cv], E. Vercellin [cy], S. Vergara [ce], R. Vernet [w,31], M. Verweij [da], I. Vetlitskiy [bn], L. Vickovic [cr], G. Viesti [bz], O. Vikhlyantsev [co], Z. Vilakazi [v], O. Villalobos Baillie [l], A. Vinogradov [bp], L. Vinogradov [cs], Y. Vinogradov [co], T. Virgili [ck], Y.P. Viyogi [ba], A. Vodopianov [ah], K. Voloshin [bn], S. Voloshin [ag], G. Volpe [e], B. von Haller [an], D. Vranic [ae], J. Vrláková [bc], B. Vulpescu [z], B. Wagner [h], V. Wagner [cb], L. Wallet [an], R. Wan [dg,12], D. Wang [dg], Y. Wang [ar], Y. Wang [dg], K. Watanabe [cx], Q. Wen [g], J. Wessels [br], U. Westerhoff [br], J. Wiechula [ar], J. Wikne [by], A. Wilk [br], G. Wilk [dc], M.C.S. Williams [n], N. Willis [bx], B. Windelband [ar], C. Xu [dg], C. Yang [dg], H. Yang [ar], S. Yasnopolskiy [bp], F. Yermia [bs], J. Yi [cf], Z. Yin [dg], H. Yokoyama [cx], I.-K. Yoo [cf], X. Yuan [dg,32], V. Yurevich [ah], I. Yushmanov [bp], E. Zabrodin [by], B. Zagreev [bn], A. Zalite [am], C. Zampolli [an,33], Yu. Zanevsky [ah], S. Zaporozhets [ah], A. Zarochentsev [cs], P. Závada [cc], H. Zbroszczyk [dd], P. Zelnicek [aq], A. Zenin [cd], A. Zepeda [bl], I. Zgura [p], M. Zhalov [am], X. Zhang [dg,1], D. Zhou [dg], S. Zhou [g], J. Zhu [dg], A. Zichichi [m,20], A. Zinchenko [ah], G. Zinovjev [ax], Y. Zoccarato [db], V. Zychácek [cb], M. Zynovyev [ax]

[a] *Dipartimento di Scienze e Tecnologie Avanzate dell'Università del Piemonte Orientale and Gruppo Collegato INFN, Alessandria, Italy*
[b] *Department of Physics Aligarh Muslim University, Aligarh, India*
[c] *Nikhef, National Institute for Subatomic Physics, Amsterdam, Netherlands*
[d] *Physics Department, University of Athens, Athens, Greece*
[e] *Dipartimento Interateneo di Fisica 'M. Merlin' and Sezione INFN, Bari, Italy*
[f] *Sezione INFN, Bari, Italy*
[g] *China Institute of Atomic Energy, Beijing, China*
[h] *Department of Physics and Technology, University of Bergen, Bergen, Norway*
[i] *Faculty of Engineering, Bergen University College, Bergen, Norway*
[j] *Lawrence Berkeley National Laboratory, Berkeley, CA, United States*
[k] *Institute of Physics, Bhubaneswar, India*
[l] *School of Physics and Astronomy, University of Birmingham, Birmingham, United Kingdom*
[m] *Dipartimento di Fisica dell'Università and Sezione INFN, Bologna, Italy*
[n] *Sezione INFN, Bologna, Italy*
[o] *Faculty of Mathematics, Physics and Informatics, Comenius University, Bratislava, Slovakia*
[p] *Institute of Space Sciences (ISS), Bucharest, Romania*
[q] *National Institute for Physics and Nuclear Engineering, Bucharest, Romania*
[r] *KFKI Research Institute for Particle and Nuclear Physics, Hungarian Academy of Sciences, Budapest, Hungary*
[s] *Dipartimento di Fisica dell'Università and Sezione INFN, Cagliari, Italy*
[t] *Sezione INFN, Cagliari, Italy*
[u] *Universidade Estadual de Campinas (UNICAMP), Campinas, Brazil*
[v] *Physics Department, University of Cape Town, iThemba Laboratories, Cape Town, South Africa*
[w] *Dipartimento di Fisica e Astronomia dell'Università and Sezione INFN, Catania, Italy*
[x] *Sezione INFN, Catania, Italy*
[y] *Physics Department, Panjab University, Chandigarh, India*
[z] *Laboratoire de Physique Corpusculaire (LPC), Clermont Université, Université Blaise Pascal, CNRS-IN2P3, Clermont-Ferrand, France*
[aa] *Department of Physics, Ohio State University, Columbus, OH, United States*
[ab] *Niels Bohr Institute, University of Copenhagen, Copenhagen, Denmark*
[ac] *The Henryk Niewodniczanski Institute of Nuclear Physics, Polish Academy of Sciences, Cracow, Poland*
[ad] *Universidad Autónoma de Sinaloa, Culiacán, Mexico*
[ae] *Research Division and ExtreMe Matter Institute EMMI, GSI Helmholtzzentrum für Schwerionenforschung, Darmstadt, Germany*
[af] *Institut für Kernphysik, Technische Universität Darmstadt, Darmstadt, Germany*
[ag] *Wayne State University, Detroit, MI, United States*
[ah] *Joint Institute for Nuclear Research (JINR), Dubna, Russia*
[ai] *Frankfurt Institute for Advanced Studies, Johann Wolfgang Goethe-Universität Frankfurt, Frankfurt, Germany*
[aj] *Institut für Kernphysik, Johann Wolfgang Goethe-Universität Frankfurt, Frankfurt, Germany*
[ak] *Laboratori Nazionali di Frascati, INFN, Frascati, Italy*
[al] *Gangneung-Wonju National University, Gangneung, South Korea*
[am] *Petersburg Nuclear Physics Institute, Gatchina, Russia*
[an] *European Organization for Nuclear Research (CERN), Geneva, Switzerland*
[ao] *Laboratoire de Physique Subatomique et de Cosmologie (LPSC), Université Joseph Fourier, CNRS-IN2P3, Institut Polytechnique de Grenoble, Grenoble, France*
[ap] *Centro de Aplicaciones Tecnológicas y Desarrollo Nuclear (CEADEN), Havana, Cuba*
[aq] *Kirchhoff-Institut für Physik, Ruprecht-Karls-Universität Heidelberg, Heidelberg, Germany*
[ar] *Physikalisches Institut, Ruprecht-Karls-Universität Heidelberg, Heidelberg, Germany*
[as] *Hiroshima University, Hiroshima, Japan*
[at] *University of Houston, Houston, TX, United States*

[au] *Physics Department, University of Rajasthan, Jaipur, India*
[av] *Physics Department, University of Jammu, Jammu, India*
[aw] *Helsinki Institute of Physics (HIP) and University of Jyväskylä, Jyväskylä, Finland*
[ax] *Bogolyubov Institute for Theoretical Physics, Kiev, Ukraine*
[ay] *University of Tennessee, Knoxville, TN, United States*
[az] *Saha Institute of Nuclear Physics, Kolkata, India*
[ba] *Variable Energy Cyclotron Centre, Kolkata, India*
[bb] *Fachhochschule Köln, Köln, Germany*
[bc] *Faculty of Science, P.J. Šafárik University, Košice, Slovakia*
[bd] *Institute of Experimental Physics, Slovak Academy of Sciences, Košice, Slovakia*
[be] *Laboratori Nazionali di Legnaro, INFN, Legnaro, Italy*
[bf] *Sección Física, Departamento de Ciencias, Pontificia Universidad Católica del Perú, Lima, Peru*
[bg] *Lawrence Livermore National Laboratory, Livermore, CA, United States*
[bh] *Division of Experimental High Energy Physics, University of Lund, Lund, Sweden*
[bi] *Centro de Investigaciones Energéticas Medioambientales y Tecnológicas (CIEMAT), Madrid, Spain*
[bj] *Instituto de Ciencias Nucleares, Universidad Nacional Autónoma de México, Mexico City, Mexico*
[bk] *Instituto de Física, Universidad Nacional Autónoma de México, Mexico City, Mexico*
[bl] *Centro de Investigación y de Estudios Avanzados (CINVESTAV), Mexico City and Mérida, Mexico*
[bm] *Institute for Nuclear Research, Academy of Sciences, Moscow, Russia*
[bn] *Institute for Theoretical and Experimental Physics, Moscow, Russia*
[bo] *Moscow Engineering Physics Institute, Moscow, Russia*
[bp] *Russian Research Centre Kurchatov Institute, Moscow, Russia*
[bq] *Indian Institute of Technology, Mumbai, India*
[br] *Institut für Kernphysik, Westfälische Wilhelms-Universität Münster, Münster, Germany*
[bs] *SUBATECH, Ecole des Mines de Nantes, Université de Nantes, CNRS-IN2P3, Nantes, France*
[bt] *Yale University, New Haven, CT, United States*
[bu] *Budker Institute for Nuclear Physics, Novosibirsk, Russia*
[bv] *Oak Ridge National Laboratory, Oak Ridge, TN, United States*
[bw] *Physics Department, Creighton University, Omaha, NE, United States*
[bx] *Institut de Physique Nucléaire d'Orsay (IPNO), Université Paris-Sud, CNRS-IN2P3, Orsay, France*
[by] *Department of Physics, University of Oslo, Oslo, Norway*
[bz] *Dipartimento di Fisica dell'Università and Sezione INFN, Padova, Italy*
[ca] *Sezione INFN, Padova, Italy*
[cb] *Faculty of Nuclear Sciences and Physical Engineering, Czech Technical University in Prague, Prague, Czech Republic*
[cc] *Institute of Physics, Academy of Sciences of the Czech Republic, Prague, Czech Republic*
[cd] *Institute for High Energy Physics, Protvino, Russia*
[ce] *Benemérita Universidad Autónoma de Puebla, Puebla, Mexico*
[cf] *Pusan National University, Pusan, South Korea*
[cg] *Nuclear Physics Institute, Academy of Sciences of the Czech Republic, Řež u Prahy, Czech Republic*
[ch] *Dipartimento di Fisica dell'Università 'La Sapienza' and Sezione INFN, Rome, Italy*
[ci] *Sezione INFN, Rome, Italy*
[cj] *Commissariat à l'Energie Atomique, IRFU, Saclay, France*
[ck] *Dipartimento di Fisica 'E.R. Caianiello' dell'Università and Sezione INFN, Salerno, Italy*
[cl] *California Polytechnic State University, San Luis Obispo, CA, United States*
[cm] *Departamento de Física de Partículas and IGFAE, Universidad de Santiago de Compostela, Santiago de Compostela, Spain*
[cn] *Universidade de São Paulo (USP), São Paulo, Brazil*
[co] *Russian Federal Nuclear Center (VNIIEF), Sarov, Russia*
[cp] *Department of Physics, Sejong University, Seoul, South Korea*
[cq] *Yonsei University, Seoul, South Korea*
[cr] *Technical University of Split FESB, Split, Croatia*
[cs] *V. Fock Institute for Physics, St. Petersburg State University, St. Petersburg, Russia*
[ct] *Institut Pluridisciplinaire Hubert Curien (IPHC), Université de Strasbourg, CNRS-IN2P3, Strasbourg, France*
[cu] *University of Tokyo, Tokyo, Japan*
[cv] *Dipartimento di Fisica dell'Università and Sezione INFN, Trieste, Italy*
[cw] *Sezione INFN, Trieste, Italy*
[cx] *University of Tsukuba, Tsukuba, Japan*
[cy] *Dipartimento di Fisica Sperimentale dell'Università and Sezione INFN, Turin, Italy*
[cz] *Sezione INFN, Turin, Italy*
[da] *Nikhef, National Institute for Subatomic Physics and Institute for Subatomic Physics of Utrecht University, Utrecht, Netherlands*
[db] *Université de Lyon, Université Lyon 1, CNRS-IN2P3, IPN-Lyon, Villeurbanne, France*
[dc] *Soltan Institute for Nuclear Studies, Warsaw, Poland*
[dd] *Warsaw University of Technology, Warsaw, Poland*
[de] *Purdue University, West Lafayette, IN, United States*
[df] *Zentrum für Technologietransfer und Telekommunikation (ZTT), Fachhochschule Worms, Worms, Germany*
[dg] *Hua-Zhong Normal University, Wuhan, China*
[dh] *Yerevan Physics Institute, Yerevan, Armenia*
[di] *Rudjer Bošković Institute, Zagreb, Croatia*

* Corresponding author.
E-mail address: appels@ikf.uni-frankfurt.de (H. Appelshäuser).
[1] Also at Laboratoire de Physique Corpusculaire (LPC), Clermont Université, Université Blaise Pascal, CNRS-IN2P3, Clermont-Ferrand, France.
[2] Also at Frankfurt Institute for Advanced Studies, Johann Wolfgang Goethe-Universität Frankfurt, Frankfurt, Germany.
[3] Now at Sezione INFN, Padova, Italy.
[4] Now at Research Division and ExtreMe Matter Institute EMMI, GSI Helmholtzzentrum für Schwerionenforschung, Darmstadt, Germany.
[5] Now at Institut für Kernphysik, Johann Wolfgang Goethe-Universität Frankfurt, Frankfurt, Germany.
[6] Now at Physics Department, University of Cape Town, iThemba Laboratories, Cape Town, South Africa.

[7] Now at National Institute for Physics and Nuclear Engineering, Bucharest, Romania.

[8] Also at University of Houston, Houston, TX, United States.

[9] Now at Faculty of Science, P.J. Šafárik University, Košice, Slovakia.

[10] Now at European Organization for Nuclear Research (CERN), Geneva, Switzerland.

[11] Now at Helsinki Institute of Physics (HIP) and University of Jyväskylä, Jyväskylä, Finland.

[12] Now at Institut Pluridisciplinaire Hubert Curien (IPHC), Université de Strasbourg, CNRS-IN2P3, Strasbourg, France.

[13] Now at Institut für Kernphysik, Westfälische Wilhelms-Universität Münster, Münster, Germany.

[14] Now at University of Technology and Austrian Academy of Sciences, Vienna, Austria.

[15] Also at Lawrence Livermore National Laboratory, Livermore, CA, United States.

[16] Also at European Organization for Nuclear Research (CERN), Geneva, Switzerland.

[17] Deceased.

[18] Now at Yale University, New Haven, CT, United States.

[19] Now at University of Tsukuba, Tsukuba, Japan.

[20] Also at Centro Fermi – Centro Studi e Ricerche e Museo Storico della Fisica "Enrico Fermi", Rome, Italy.

[21] Also at Laboratoire de Physique Subatomique et de Cosmologie (LPSC), Université Joseph Fourier, CNRS-IN2P3, Institut Polytechnique de Grenoble, Grenoble, France.

[22] Now at Dipartimento di Fisica Sperimentale dell'Università and Sezione INFN, Turin, Italy.

[23] Now at Commissariat à l'Energie Atomique, IRFU, Saclay, France.

[24] Also at Department of Physics, University of Oslo, Oslo, Norway.

[25] Now at Physikalisches Institut, Ruprecht-Karls-Universität Heidelberg, Heidelberg, Germany.

[26] Now at Department of Physics and Technology, University of Bergen, Bergen, Norway.

[27] Now at Physics Department, University of Athens, Athens, Greece.

[28] Also at Institut für Kernphysik, Westfälische Wilhelms-Universität Münster, Münster, Germany.

[29] Now at SUBATECH, Ecole des Mines de Nantes, Université de Nantes, CNRS-IN2P3, Nantes, France.

[30] Now at Université de Lyon, Université Lyon 1, CNRS-IN2P3, IPN-Lyon, Villeurbanne, France.

[31] Now at Centre de Calcul IN2P3, Lyon, France.

[32] Also at Dipartimento di Fisica dell'Università and Sezione INFN, Padova, Italy.

[33] Also at Sezione INFN, Bologna, Italy.

[34] Also at Dipartimento di Fisica dellÚniversità, Udine, Italy.

[35] Also at Wrocław University, Wrocław, Poland.

[36] Now at Dipartimento di Fisica dell'Università and Sezione INFN, Padova, Italy.